

Contents lists available at ScienceDirect

Petroleum Science

journal homepage: www.keaipublishing.com/en/journals/petroleum-science



Original Paper

Monitoring the change in horizontal stress with multi-wave timelapse seismic response based on nonlinear elasticity theory



Fu-Bin Chen a, b, c, Zhao-Yun Zong a, b, c, *, Xing-Yao Yin a, b, c

- ^a School of Geosciences, China University of Petroleum East China, Qingdao, Shandong, 266580, China
- ^b Laoshan Laboratory, Qingdao, Shandong, 266580, China
- ^c Shandong Provincial Key Laboratory of Deep Oil and Gas, Qingdao, Shandong, 266580, China

ARTICLE INFO

Article history: Received 11 April 2022 Received in revised form 11 August 2022 Accepted 20 September 2022 Available online 24 September 2022

Edited by Jie Hao

Keywords:
Monitoring change in horizontal stress
Multi-wave reflection coefficients
Nonlinear elasticity theory
Time-lapse seismic data

ABSTRACT

Monitoring the change in horizontal stress from the geophysical data is a tough challenge, and it has a crucial impact on broad practical scenarios which involve reservoir exploration and development, carbon dioxide (CO₂) injection and storage, shallow surface prospecting and deep-earth structure description. The change in in-situ stress induced by hydrocarbon production and localized tectonic movements causes the changes in rock mechanic properties (e.g. wave velocities, density and anisotropy) and further causes the changes in seismic amplitudes, phases and travel times. In this study, the nonlinear elasticity theory that regards the rock skeleton (solid phase) and pore fluid as an effective whole is used to characterize the effect of horizontal principal stress on rock overall elastic properties and the stressdependent anisotropy parameters are therefore formulated. Then the approximate P-wave, SV-wave and SH-wave angle-dependent reflection coefficient equations for the horizontal-stress-induced anisotropic media are proposed. It is shown that, on the different reflectors, the stress-induced relative changes in reflectivities (i.e., relative difference) of elastic parameters (i.e., P- and S-wave velocities and density) are much less than the changes in contrasts of anisotropy parameters. Therefore, the effects of stress change on the reflectivities of three elastic parameters are reasonably neglected to further propose an AVO inversion approach incorporating P-, SH- and SV-wave information to estimate the change in horizontal principal stress from the corresponding time-lapse seismic data. Compared with the existing methods, our method eliminates the need for man-made rock-physical or fitting parameters, providing more stable predictive power. 1D test illustrates that the estimated result from time-lapse P-wave reflection data shows the most reasonable agreement with the real model, while the estimated result from SH-wave reflection data shows the largest bias. 2D test illustrates the feasibility of the proposed inversion method for estimating the change in horizontal stress from P-wave time-lapse seismic data. © 2022 The Authors, Publishing services by Elsevier B.V. on behalf of KeAi Communications Co. Ltd. This is an open access article under the CC BY-NC-ND license (http://creativecommons.org/licenses/by-nc-nd/ 4.0/).

1. Introduction

The in-situ stress changes in the subsurface are usually caused by several engineering productions which involve oil and gas exploration, CO₂ injection and mining, some natural activities such as natural dissolution and localized tectonic movement (House et al., 2006; Tromp and Trampert, 2018; Chen et al., 2021; Sripanich et al., 2021; Li et al., 2022; Cai et al., 2022). The information on changes in stress has practical applications in better

E-mail address: zongzhaoyun@126.com (Z.-Y. Zong).

understanding the changes in the geofluid, barriers, compartments and faults. In addition, monitoring the changes in in-situ stress can distinguish the abnormal high-stress circumstances that helps to timely adjust the mud concentration to avoid blowout accidents during drilling (Wong, 2017).

In-situ stress affects the rock structure to significantly change the macroscopic rock properties, which influences the wave propagation in the subsurface Earth (Winkler and McGowan, 2004; Chen et al., 2021, 2022a, 2022b). Generally, the elevating applied stress can compact the porous rock to increase its wave velocities within the elastic limitation (Winkler and McGowan, 2004). This further causes the changes in seismic amplitudes, phases and travel times. Some important rock elastic parameters which can be

 $[\]ast$ Corresponding author. School of Geosciences, China University of Petroleum East China, Qingdao, Shandong, 266580, China.

inverted from seismic data, such as P- and S-wave impedances and the ratio of P- to S-wave velocities, are effective indicators to describe the stress changes in specific field areas (Tura and Lumley, 1999; Rojas et al., 2005). These empirical and semi-quantitative approaches based on rock physics analysis or well-logging observation are greatly powerful tools in field production. Time-lapse seismic data from baseline time to monitor survey time incorporates the information on the change in in-situ stress over the production period, and it can be used to estimate the change in stress (Landrø, 2001). Based on the effect of stress on seismic travel times, Landrø (2001) introduced six regression coefficients to construct the formulas for representing the changes in seismic AVO intercept and slope in terms of the changes in stress and saturation. With these quantitative formulas, the changes in stress and saturation are estimated with time-lapse seismic data after the six coefficients are determined from the calibrated well-logging data. To render more accurate results, Meadows (2001) added the quadratic saturation terms as well, in addition to the linear terms, to expand the Landrø model. Then Grude and Landrø (2012) performed Landrø model (2001) to discriminate the changes in stress and saturation induced by CO2 injection, and they found this method provided over-estimated results. Lang and Grana (2019) utilized the rock physics model to rearrange the Landrø model and Meadows model to propose the corresponding novel stress estimation equations in terms of the initial porosity, stress and saturation, with some additional fitting coefficients. Despite the reasonable estimated results achieved, the schemes for stress estimation with these novel equations become very complicated due to the additional fitting coefficients and rock physical parameters. Moreover, Trani et al. (2011) considered the effect of stress on the seismic time shifts to calibrate the Meadows model, which helps reduce the uncertainty of quantifying the change in stress. The good estimated results can be obtained with the methods mentioned above if the initial porosity field is known, but inverting the porosity in the subsurface media from the seismic data still is a challenge. Afterwards, Witsker et al. (2014) combined the Gassmann rock-physics model and Hertz-Mindlin model to propose a pseudo-steadystate engineering flow equation to model the first-order influence of the stress change on time-lapse seismic, avoiding the considerable computing time. Stovas and Landrø (2004) utilized the joint information of the P wave and SV wave to calculate the stress change. This operation illustrates the potential for estimating the stress change with the information of multi waves. In this study, we will propose a novel method to estimate the stress change with the multi-waves time-lapse reflection data.

Despite the efforts in theoretical research and practical applications with the empirical and fitting methods made over the years, the man-made determination of suitable fitting coefficients remains a challenge, and the ill-suited fitting coefficients embedded in the existing methods produce strong uncertainty in the results. Quantifying and estimating the change in in-situ stress from the observed seismic signals is still difficult due to the lack of physical relationship between the change in stress and wave reflection coefficients (Landrø, 2001; Trani et al., 2011; Lang and Grana, 2019).

An alternative model that describes the effect of stress on rock overall properties is nonlinear elasticity theory, also named third-order elasticity (TOE) theory and acoustoelasticity theory (Hughes and Kelly, 1953; Thurston and Brugger, 1964; Chen et al., 2022a). This theory holds the rock skeleton and the permeated fluid as an effective whole and introduces three TOE moduli to describe its stress dependence, excluding the empirical or fitting parameters. Therefore, the stress-dependent rock overall elasticity can be characterized with this theory without considering the characteristics of the rock interior, such as the fluid properties (e.g., saturation, fluidity) and microscopic pore structure (pore aspect ratio,

tortuosity, and roughness of inner pore wall). It has broad practical applications in nondestructive testing (Masumi et al., 2010), wave propagation evaluation (Degtyar and Rokhlin, 1998; Liu et al., 2012; Chen et al., 2021, 2022b), third-order elastic constants estimation (Winkler and McGowan, 2004) and stress-induced anisotropy analysis (Sarkar et al., 2003; Liu et al., 2017). From the perspective of rock physics, the stress-induced anisotropy is induced by the closure of the cracks perpendicular to the stress axis before that along the stress axis direction (Johnson and Rasolofosaon, 1996). Considerable theoretical (Rasolofosaon, 1998; Shapiro, 2017) and laboratory research (Nur and Simmons, 1969; Sarkar et al., 2003) on stress-induced anisotropy has been carried out. Sarkar et al. (2003) proposed a relatively simple but useful model to link the applied stress and rock Thomsen anisotropy parameters (Thomsen, 1986) in the context of the nonlinear elasticity theory. This model is validated under the limited (weak and moderate) applied stresses (Sarkar et al., 2003; Liu et al., 2017).

In this study, the nonlinear elasticity theory is used to investigate the effect of horizontal stress on the wave reflection coefficient and to quantitatively estimate horizontal stress from the seismic data. We first revisit the nonlinear elasticity theory and the relationship between the rock mechanic properties (P- and S-wave velocities, density and anisotropy parameters) and horizontal principal stress. Then the stress-induced changes in reflectivities (i.e., relative difference) of elastic parameters (P- and S-wave velocities and density) are reasonably neglected to propose six equations for estimating the change in horizontal stress from multi-wave (P, SH and SV waves) time-lapse seismic reflection data based on the nonlinear elasticity theory, wave reflection theory and stress-induced anisotropy model, without any additional empirical or fitting coefficients. Finally, the proposed inversion method is implemented on the synthetic 1D and 2D cases to illustrate its robustness and feasibility.

2. Relationship between change in horizontal stress and reflection coefficients

2.1. Stress-dependent elastic stiffness tensor

In-situ stresses in the subsurface Earth usually change with engineering and natural activities. The existing literature suggests that the vertical overburden changes much more minor than horizontal stress in a short temporal period (within hundreds of years) in normal circumstances (Liu et al., 2017). Thus, we assume that only horizontal principal stress changes in the target area from the

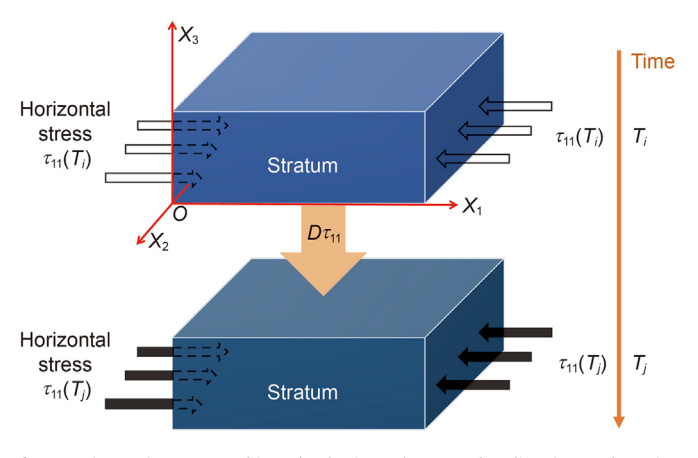


Fig. 1. An isotropic stratum subjected to horizontal stress at baseline time and monitor survey time.

baseline time T_i (the first seismic survey time) to the monitor survey time T_j , as shown in Fig. 1. Based on the nonlinear elasticity theory, the effective stiffness tensor in the isotropic medium under the effect of horizontal stress is approximately given by (Thurston and Brugger, 1964; Liu et al., 2017)

$$H_{ijkl} = c_{ijkl} + c_{ijklmn}e^{i}_{mn} \tag{1}$$

where c_{ijkl} and c_{ijklmn} are the second-order elastic (SOE) moduli and third-order elastic (TOE) moduli, respectively, with i, j, k, l, m, n = 1, 2, 3. e_{mn}^i is the initial strain tensor induced by horizontal principal stress, given by

$$\begin{bmatrix} e_{11}^{i} \\ e_{22}^{i} \\ e_{33}^{i} \\ e_{13}^{i} \\ e_{13}^{i} \\ e_{12}^{i} \end{bmatrix} = \begin{bmatrix} \lambda + 2\mu & \lambda & \lambda & 0 & 0 & 0 \\ \lambda & \lambda + 2\mu & \lambda & 0 & 0 & 0 \\ \lambda & \lambda & \lambda + 2\mu & 0 & 0 & 0 \\ 0 & 0 & 0 & \mu & 0 & 0 \\ 0 & 0 & 0 & 0 & \mu & 0 \\ 0 & 0 & 0 & 0 & 0 & \mu \end{bmatrix}^{-1} \begin{bmatrix} \tau_{11} \\ 0 \\ 0 \\ 0 \\ 0 \end{bmatrix}$$
(2)

where au_{11} is the horizontal principal stress along coordinate axis X_1 , e_{11}^i , e_{22}^i and e_{33}^i are principal strains along the corresponding axis direction X_1 , X_2 and X_3 respectively. e_{23}^i , e_{13}^i and e_{12}^i are shear strains, and they will be zero when only τ_{11} exists. The signs of compressive and tensile stresses are negative and positive, respectively, if not specified in this study. The concise Voigt notation is adopted to contract the subscripts of SOE and TOE moduli, and then H_{ijkl} , c_{ijkl} and c_{ijklmn} are written as H_{IJ} , c_{IJ} and c_{IJK} , respectively, with I,J,K = 1,2,3,4,5,6. In an isotropic medium, the SOE moduli are characterized by two independent Lamé constants λ and μ , and $c_{11} = c_{22} = c_{33} = \lambda + 2\mu$, $c_{44} = c_{55} = c_{66} = \mu$, $c_{12} = c_{44} = c_{44$ $c_{13} = c_{23} = \lambda$. $\lambda = \rho \alpha^2 - 2\rho \beta^2$ and $\mu = \rho \beta^2$ where α and β are the velocities of P- and S-wave vertically incident the upper surface of the medium, respectively. In addition, three independent TOE moduli are c_{111} , c_{112} and c_{123} , and the other TOE moduli can be computed with the relationship among them such as $c_{144} =$ $\left(c_{112}-c_{123}
ight)/2$ and $c_{155}=\left(c_{111}-c_{112}
ight)/4$, the detailed description can be found in Pao et al. (1984) and Chen et al. (2022b).

Therefore, the elements of effective elastic stiffness tensor in a stressed isotropic medium are given by

$$H_{11} = \lambda + 2\mu + c_{111}e_{11}^{i} + 2c_{112}e_{22}^{i}$$
(3)

$$H_{22} = H_{33} = \lambda + 2\mu + c_{112}e_{11}^{i} + (c_{111} + c_{112})e_{22}^{i}$$
(4)

$$H_{12} = H_{13} = \lambda + c_{112}e_{11}^{i} + (c_{123} + c_{112})e_{22}^{i}$$
(5)

$$H_{44} = \mu + c_{144}e_{11}^i + 2c_{155}e_{22}^i \tag{6}$$

$$H_{55} = H_{66} = \mu + c_{155}e_{11}^{i} + (c_{144} + c_{155})e_{22}^{i}$$

$$\tag{7}$$

$$H_{23} = H_{33} - 2H_{44} \tag{8}$$

From Eqs. (3)–(8), the stress-dependent elastic stiffness is characterized by five independent elements, that is, H_{11} , H_{33} , H_{12} , H_{44} and H_{55} . This illustrates that an isotropic medium subjected to horizontal stress approximately possesses the elastic characteristics of a horizontally transverse isotropic (i.e., HTI) medium. The

isotropic medium subjected to the horizontal principal stress can be regarded as the stress-induced anisotropic (HTI) medium.

2.2. Stress-dependent elastic anisotropy parameters

Based on Thomsen (1986), Rasolofosaon (1998) and Sarkar et al. (2003), the anisotropy parameters in a horizontal-stress-induced HTI medium are given by

$$\varepsilon^{(v)} = \xi \tau_{11} \tag{9}$$

$$\delta^{(v)} = \xi \tau_{11} \tag{10}$$

$$\gamma = -\varsigma \tau_{11} \tag{11}$$

$$\alpha = \sqrt{H_{33}/\rho^i} \tag{12}$$

$$\beta = \sqrt{H_{44}/\rho^i} \tag{13}$$

where

$$\xi = \frac{c_{111} - c_{112}}{4M\mu} \tag{14}$$

$$\varsigma = \frac{c_{111} - 3c_{112} + 2c_{123}}{16u^2} \tag{15}$$

 $\varepsilon^{(v)}$, $\delta^{(v)}$ and γ are anisotropy parameters in a horizontal stress-induced anisotropic medium, and their physical meanings refer to Thomsen (1986) and Tsvankin (1997). ρ^i is the density of a stressed isotropic medium. Based on the law of energy conservation, ρ^i is written as

$$\rho^{i} \approx \rho_{0} \left(1 - e_{11}^{i} - e_{22}^{i} - e_{33}^{i} \right) \tag{16}$$

From Eq. (16), the change in density induced by applied horizontal stress is greatly small due to the tiny rock strains and can be neglected in field applications. Utilizing Eqs. (9)-(16), the velocities, density and anisotropy parameters in the target area at any monitor survey time (i.e., any horizontal stress state) can be obtained.

2.3. Parameterization for change in wave reflection coefficients

From the Rüger (1996, 1998), the linearized P-wave, SV-wave and SH-wave reflection coefficient equations in the horizontal-stress-induced HTI media are

$$R_{p} = \frac{1}{2} \frac{\Delta I_{p}}{I_{p}} + \frac{1}{2} \left[\frac{\Delta \alpha}{\alpha} - 4k^{2} \left(2 \frac{\Delta \beta}{\beta} + \frac{\Delta \rho}{\rho} \right) + \left(\Delta \delta^{(\nu)} + 8k^{2} \Delta \gamma \right) \cos^{2} \varphi \right] \sin^{2} \theta$$
(17)

$$R_{SV}^{0} = -\frac{1}{2} \left(\frac{\Delta \beta}{\beta} + \frac{\Delta \rho}{\rho} - \Delta \gamma \right) + \begin{bmatrix} \frac{7}{2} \left(\frac{\Delta \beta}{\beta} - \Delta \gamma \right) + 2 \frac{\Delta \rho}{\rho} \\ + \frac{1}{2} \left(\frac{1}{k} \right)^{2} \left(\Delta \varepsilon^{(\nu)} - \Delta \delta^{(\nu)} \right) \end{bmatrix} \sin^{2} \theta$$
(18)

$$R_{SV}^{90} = -\frac{1}{2} \left(\frac{\Delta \beta}{\beta} + \frac{\Delta \rho}{\rho} \right) + \frac{7}{2} \left(\frac{\Delta \beta}{\beta} + 2 \frac{\Delta \rho}{\rho} \right) \sin^2 \theta \tag{19}$$

$$R_{SH}^{0} = -\frac{1}{2} \left(\frac{\Delta \beta}{\beta} + \frac{\Delta \rho}{\rho} \right) + \frac{1}{2} \left(\frac{\Delta \beta}{\beta} - \Delta \gamma \right) \tan^{2} \theta \tag{20}$$

$$R_{SH}^{90} = -\frac{1}{2} \left(\frac{\Delta \beta}{\beta} + \frac{\Delta \rho}{\rho} - \varDelta \gamma \right) + \frac{1}{2} \left(\frac{\Delta \beta}{\beta} - \varDelta \gamma \right) tan^2 \ \theta \tag{21}$$

where the superscripts "0" and "90" represent the azimuths of 0° and 90° , respectively. The elastic parameters $(\alpha, \beta \text{ and } \rho)$ and anisotropy parameters ($\varepsilon^{(\nu)}$, $\delta^{(\nu)}$ and γ) in Eqs. (17)–(21) are stressdependent which can be computed by Eqs. (9)–(13). k is the ratio of average S-wave velocity to P-wave velocity of two unstressed isotropic media, $k = \beta/\alpha$. θ is the incident angle measured from vertical axis and φ is the azimuth angle. $\Delta \alpha$, $\Delta \beta$, $\Delta \rho$, ΔI_p and $\Delta \varepsilon^{(v)}$, $\Delta\delta^{(
u)}$, $\Delta\gamma$ are the differences of the corresponding parameters across the interface. $\Delta \alpha/\alpha$, $\Delta \beta/\beta$, $\Delta \rho/\rho$ and $\Delta I_p/I_p$ are P-wave velocity reflectivity (i.e., relative difference), S-wave velocity reflectivity, density reflectivity and P-wave impedance reflectivity, respectively, where α , β , ρ and I_p are average P-wave velocity, S-wave velocity, density and P-wave impedance of two unstressed isotropic media, respectively. Furthermore, combining Eqs. (17)-(21), P-wave, SVwave and SH-wave reflection coefficient equations in the HTI medium at the monitor survey time T_i are given by

$$\begin{split} R_{p}(T_{i}) &= \frac{1}{2} \frac{\Delta I_{p}}{I_{p}}(T_{i}) \\ &+ \frac{1}{2} \left\{ \frac{\Delta \alpha}{\alpha} (T_{i}) - 2k(T_{i})^{2} \left(2 \frac{\Delta \beta}{\beta} (T_{i}) + \frac{\Delta \rho}{\rho} (T_{i}) \right) \right. \\ &+ \left[\Delta \delta^{(\nu)}(T_{i}) + 8k(T_{i})^{2} \Delta \gamma(T_{i}) \right] \cos^{2} \varphi \end{split} \right\} \sin^{2} \theta \end{split}$$

$$(22)$$

$$R_{SV}^{0}(T_{i}) = -\frac{1}{2} \begin{bmatrix} \frac{\Delta\beta}{\beta}(T_{i}) + \frac{\Delta\rho}{\rho}(T_{i}) \\ -\Delta\gamma(T_{i}) \end{bmatrix} + \begin{cases} \frac{7}{2} \left[\frac{\Delta\beta}{\beta}(T_{i}) - \Delta\gamma(T_{i}) \right] + 2\frac{\Delta\rho}{\rho}(T_{i}) \\ +\frac{1}{2} \left(\frac{1}{k} \right)^{2} \left[\Delta\varepsilon^{(\nu)}(T_{i}) - \Delta\delta^{(\nu)}(T_{i}) \right] \end{cases} \sin^{2}\theta$$
 (23)

$$R_{SV}^{90}(T_i) = -\frac{1}{2} \left(\frac{\Delta \beta}{\beta}(T_i) + \frac{\Delta \rho}{\rho}(T_i) \right) + \frac{7}{2} \left(\frac{\Delta \beta}{\beta}(T_i) + 2 \frac{\Delta \rho}{\rho}(T_i) \right) \sin^2 \theta$$
(24)

$$R_{SH}^{0}(T_{i}) = -\frac{1}{2} \left(\frac{\Delta \beta}{\beta}(T_{i}) + \frac{\Delta \rho}{\rho}(T_{i}) \right) + \frac{1}{2} \left(\frac{\Delta \beta}{\beta}(T_{i}) - \Delta \gamma(T_{i}) \right) \tan^{2} \theta$$
(25)

$$R_{SH}^{90}(T_i) = -\frac{1}{2} \left(\frac{\Delta \beta}{\beta} (T_i) + \frac{\Delta \rho}{\rho} (T_i) - \Delta \gamma (T_i) \right) + \frac{1}{2} \left(\frac{\Delta \beta}{\beta} (T_i) - \Delta \gamma (T_i) \right) \tan^2 \theta$$
(26)

Based on the effective elastic stiffness tensor (Eq. (1)) and the horizontal stress-induced anisotropy parameters (Eqs. (3)-(8)), it is known that an isotropic medium, when horizontally stressed, can approximately perform like an HTI medium whose symmetry axis

is consistent with the direction of horizontal principal stress. Therefore, combining Eqs. (9)–(11) and Eqs. (22)–(26), the differences in P-wave, SV-wave and SH-wave reflection coefficients from baseline time to monitor survey time can be derived as

$$DR_{p} = \frac{1}{2}D\frac{\Delta I_{p}}{I_{p}} + \frac{1}{2} \left\{ D\frac{\Delta \alpha}{\alpha} - 4D\left[(k)^{2} \left(2\frac{\Delta \beta}{\beta} + \frac{\Delta \rho}{\rho} \right) \right] + \left[D\Delta(\xi \tau_{11}) - 8D\left(k^{2}\Delta(\xi \tau_{11}) \right) \right] \cos^{2} \varphi \right\} \sin^{2} \theta$$
(27)

$$\begin{split} DR_{SV}^{0} &= -\frac{1}{2} \left\{ D \frac{\Delta \beta}{\beta} + D \frac{\Delta \rho}{\rho} + D \Delta (\varsigma \tau_{11}) \right\} \\ &+ \left\{ \frac{7}{2} \left[D \frac{\Delta \beta}{\beta} + D \Delta (\varsigma \tau_{11}) \right] + 2D \frac{\Delta \rho}{\rho} \right\} \sin^{2} \theta \end{split} \tag{28}$$

$$DR_{SV}^{90} = -\frac{1}{2} \left(D \frac{\Delta \beta}{\beta} + D \frac{\Delta \rho}{\rho} \right) + \frac{7}{2} \left(D \frac{\Delta \beta}{\beta} + 2D \frac{\Delta \rho}{\rho} \right) \sin^2 \theta$$
 (29)

$$DR_{SH}^{0} = -\frac{1}{2} \left(D \frac{\Delta \beta}{\beta} + D \frac{\Delta \rho}{\rho} \right) + \frac{1}{2} \left(D \frac{\Delta \beta}{\beta} + D \Delta(\varsigma \tau_{11}) \right) tan^{2} \theta \qquad (30)$$

$$\begin{split} DR_{SH}^{90} &= -\frac{1}{2} \left(D \frac{\Delta \beta}{\beta} + D \frac{\Delta \rho}{\rho} - D \Delta (\varsigma \tau_{11}) \right) \\ &+ \frac{1}{2} \left(D \frac{\Delta \beta}{\beta} + D \Delta (\varsigma \tau_{11}) \right) \tan^2 \theta \end{split} \tag{31}$$

$$DR_{SV}^{90} - DR_{SV}^{0} = \frac{1 - 7\sin^2\theta}{2} D\Delta(\varsigma\tau_{11})$$
 (32)

$$DR_{SH}^{90} - DR_{SH}^{0} = \frac{1}{2}D\Delta(\varsigma \tau_{11})$$
 (33)

where the operator D represents the difference of the physical quantity from baseline time T_i to monitor survey time T_j , i.e. $Dx = x(T_j) - x(T_i)$. Detailed expressions for ξ and ς are shown in Eqs. (14) and (15). In the case that the horizontal stress applied to the lower medium is much larger than that applied to the upper medium, we have

$$\Delta[\varsigma\tau_{11}] \approx \varsigma\tau_{11} \tag{34}$$

In addition, we use Eqs. (9)–(13) to compute the P-wave impedance reflectivity $\Delta I_p/I_p$ (named as R-Ip in Fig. 2), P-wave velocity reflectivity $\Delta \alpha/\alpha$ (named as R-Vp in Fig. 2), S-wave velocity reflectivity $\Delta \beta/\beta$ (named as R-Vs in Fig. 2), density reflectivity $\Delta \rho/\rho$ (named as R-Density in Fig. 2) and the contrasts of anisotropy parameters across the interface $\Delta \delta^{(\nu)}$ (named as Delta in Fig. 2), $\Delta \epsilon^{(\nu)}$ (named as Epsilon in Fig. 2) and $\Delta \gamma^{(\nu)}$ (named as Gamma in Fig. 2) variation with the horizontal principal stress, as shown in Fig. 2. From Fig. 2, we have

$$D\frac{\Delta I_p}{I_p} \approx D\frac{\Delta \rho}{\rho} \approx D\frac{\Delta \beta}{\beta} \approx 0 \tag{35}$$

Substituting Eqs. (34) and (35) into Eqs. (27)-(33), yields

$$DR_{p} = \frac{\cos^{2} \varphi \sin^{2} \theta}{2} \left[D(\xi \tau_{11}) - 8k(T_{i})^{2} D(\varsigma \tau_{11}) \right]$$
 (36)

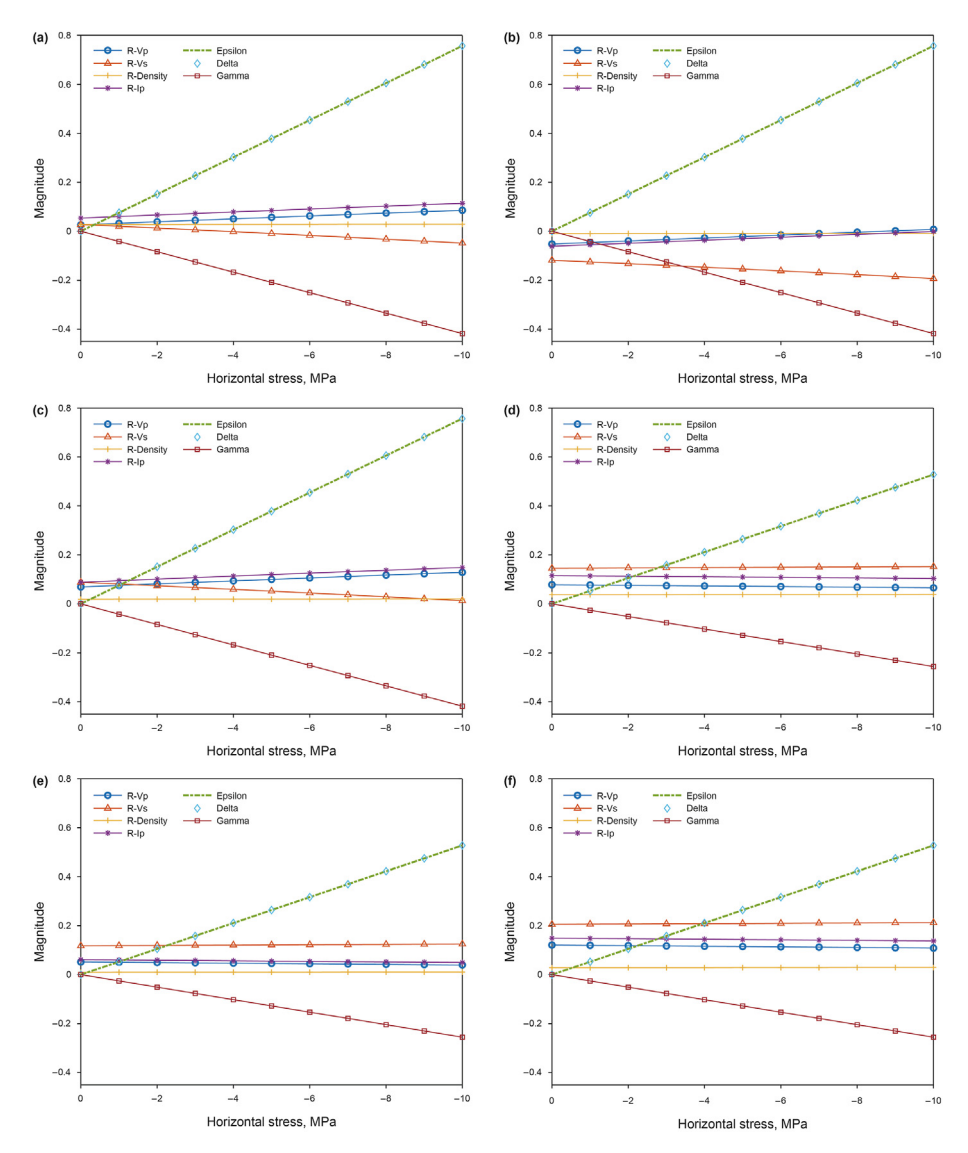


Fig. 2. The reflectivities of the elastic parameters $(\frac{\Delta \alpha}{\alpha}, \frac{\Delta \beta}{\beta}, \frac{\Delta \rho}{\rho})$ and the contrasts of anisotropy parameters $(\Delta \varepsilon^{(v)}, \Delta \delta^{(v)})$ and $\Delta \gamma$ variation with horizontal stress in different models. (a) Rock 2 overlying Rock 1. (b) Rock 2 overlying Rock 3. (c) Rock 2 overlying Rock 4. (d) Rock 3 overlying Rock 1. (e) Rock 3 overlying Rock 2. (f) Rock 3 overlying Rock 3. (e) Rock 3 overlying Rock 4. (e) Rock 3 overlying Rock 3 overlying Rock 3 overlying Rock 4. (e) Rock 3 overlying Rock 3 overlying Rock 3 overlying Rock 4. (f) Rock 3 overlying Rock 4. (e) Rock 3 overlying Rock 5 overlying Rock 5 overlying Rock 6 overlying Rock 7 overlying Rock 8 overlying Rock 9 overlyi

$$DR_{SV}^{0} = -\frac{1 - 7\sin^{2}\theta}{2}D(\varsigma\tau_{11}) \qquad (37) \qquad D(\varsigma\tau_{11}) = \varsigma D\tau_{11} + \tau_{11}(T_{i})D\varsigma = \varsigma D\tau_{11} \qquad (42)$$

$$DR_{SH}^0 = -\frac{\tan^2 \theta}{2} D(\varsigma \tau_{11}) \tag{38}$$

$$DR_{SH}^{90} = -\frac{1 - \tan^2 \theta}{2} D(\varsigma \tau_{11})$$
 (39)

$$D\left(R_{SV}^{90} - R_{SV}^{0}\right) = \frac{1 - 7\sin^{2}\theta}{2}D(\varsigma\tau_{11}) \tag{40}$$

$$D(R_{SH}^{90} - R_{SH}^{0}) = \frac{1}{2}D(\varsigma\tau_{11}) \tag{41}$$

The SOE and TOE moduli of an isotropic medium are independent of horizontal stress, leading to $\varsigma(T_i) = \varsigma(T_j) = \varsigma$, $\xi(T_i) = \xi(T_j) = \xi$ (see Eqs. (14) and (15)). Thus, we have

$$D(\xi\tau_{11}) = \xi D\tau_{11} + \tau_{11}(T_i)D\xi = \xi D\tau_{11} \tag{43}$$

Combining Eqs. (42) and (43), Eqs. (36)–(41) are rearranged as

$$DR_p = \frac{\left[\xi - 8\varsigma k(T_i)^2\right]\cos^2\varphi\sin^2\theta}{2}D\tau_{11}$$
(44)

$$DR_{SV}^{0} = -\frac{\varsigma \left(1 - 7\sin^{2}\theta\right)}{2}D\tau_{11} \tag{45}$$

$$DR_{SH}^{0} = -\frac{\varsigma \tan^{2} \theta}{2} D\tau_{11}$$
 (46)

$$DR_{SH}^{90} = -\frac{\varsigma(1 - \tan^2 \theta)}{2} D\tau_{11}$$
 (47)

$$D\left(R_{SV}^{90} - R_{SV}^{0}\right) = \frac{\varsigma\left(1 - 7\sin^{2}\theta\right)}{2}D\tau_{11}$$
 (48)

$$D(R_{SH}^{90} - R_{SH}^{0}) = \frac{\varsigma}{2} D\tau_{11} \tag{49}$$

Eqs. (44)-(49) can be utilized to estimate the change in horizontal stress from the time-lapse seismic reflection data of the P wave, 0°-azimuth SV wave, 90°-azimuth SV wave, 0°-azimuth SH wave and 90°-azimuth SH wave. Eqs. (44)-(49) will produce unavoidable errors in estimating the change in horizontal stress due to some necessary assumptions (see Eqs. (34) and (35)). Even so, they are physically based models to reveal the effect of the change in horizontal stress on the change in multi-wave reflection coefficients that help further describe the stress dependence of timelapse reflection signature (i.e., observed seismic records).

3. Time-lapse seismic AVO inversion for change in horizontal stress

Eqs. (44)–(49) represent the changes in wave reflection coefficient equations in terms of the original elastic properties at the baseline time and the change in horizontal stress. With Eqs. (44)–(49), the corresponding AVO inversion method for horizontal stress estimation is proposed. Rearranging Eqs. (44)–(49) yields the changes in wave reflection coefficients changing from baseline time to monitor survey time, given by

$$D\mathbf{R} = \mathbf{A}(\theta)D\tau_{11} \tag{50}$$

where

$$\mathbf{R} = \begin{bmatrix} R_p, & R_{SV}^0, & R_{SH}^0, & R_{SH}^{90}, & R_{SV}^{90} - R_{SV}^0, & R_{SH}^{90} - R_{SH}^0 \end{bmatrix}$$
 (51)

$$\boldsymbol{A} = \frac{1}{2} \left[\cos^2 \varphi \sin^2 \theta \left[\xi - 8 \varsigma k (T_i)^2 \right], \quad \left(7 \sin^2 \theta - 1 \right) \varsigma, \quad -\tan^2 \theta \varsigma, \quad \left(\tan^2 \theta - 1 \right) \varsigma, \quad \left(1 - 7 \sin^2 \theta \right) \varsigma, \quad \varsigma \right]$$

Then the AVO inversion method can be implemented based on Eqs. (50)–(52). This inversion approach incorporating the data of P wave, 0°-azimuth SV wave, 90°-azimuth SV wave, 0°-azimuth SH wave and 90°-azimuth SH wave are named D1, D2, D3, D4, D5 and D6, respectively, avoiding confusion in the subsequent description.

According to Eqs. (44)–(49), at least one incident angle θ_1 is required to estimate the change in horizontal stress (theoretically, more partial angle-stack seismic data can render a more accurate inversion result (Zong and Ji, 2021)). If there are Y formation interfaces in the real subsurface, we have

$$D\mathbf{R}_{Y\times 1} = \begin{bmatrix} DR^{1}(\theta_{1}) & DR^{2}(\theta_{1}) & \dots & DR^{Y}(\theta_{1}) \end{bmatrix}^{T}$$
(53)

$$\mathbf{A}_{Y\times Y} = \begin{bmatrix} A_1(\theta_1) & 0 & 0 & 0\\ 0 & A_2(\theta_1) & 0 & 0\\ 0 & 0 & \cdots & 0\\ 0 & 0 & 0 & A_Y(\theta_1) \end{bmatrix}$$
 (54)

$$D\tau_{11_{Y\times 1}} = \begin{bmatrix} D\tau_{11}^1 & D\tau_{11}^2 & \cdots & D\tau_{11}^Y \end{bmatrix}^T$$
 (55)

The seismic data at baseline time T_i and monitor time T_i synthesized by convolution model are, respectively,

$$\mathbf{S}(T_i) = \mathbf{WR}(T_i) \tag{56}$$

and

$$\mathbf{S}(T_i) = \mathbf{WR}(T_i) \tag{57}$$

Combining Eqs. (50), (56) and (57) yields

$$D\mathbf{S} = \mathbf{W}\mathbf{A}D\tau_{11} \tag{58}$$

where \mathbf{W} is a minimum-phase wavelet matrix (Zong and Ji, 2021),

$$\boldsymbol{W}_{Y\times Y}(\theta_{1}) = \begin{bmatrix} w_{Y} & 0 & 0 & 0 & 0 & 0 & 0 \\ w_{Y+1} & w_{Y} & 0 & 0 & 0 & 0 & 0 \\ \vdots & w_{Y+1} & w_{Y} & 0 & 0 & 0 & 0 & 0 \\ w_{l-1} & \vdots & w_{Y+1} & \ddots & 0 & 0 & 0 & 0 \\ w_{l} & w_{l-1} & \vdots & w_{Y+1} & w_{Y} & 0 & 0 & 0 \\ 0 & w_{l} & w_{l-1} & \vdots & w_{Y+1} & w_{Y} & 0 & 0 \\ 0 & 0 & w_{l} & w_{l-1} & \vdots & w_{Y+1} & w_{Y} & 0 \\ 0 & 0 & w_{l} & w_{l-1} & \vdots & w_{Y+1} & w_{Y} & 0 \end{bmatrix}$$

$$(59)$$

where w is wavelet function, l is wavelet length,

$$D\mathbf{S} = \begin{bmatrix} DS^{1}(\theta_{1}) & DS^{2}(\theta_{1}) & \cdots & DS^{Y}(\theta_{1}) \end{bmatrix}^{T}$$
(60)

The objective function is established in terms of the L2-norm of the misfit, given by

$$(\tan^2 \theta - 1)\varsigma, \quad (1 - 7\sin^2 \theta)\varsigma, \quad \varsigma$$
 (52)

$$J = \min \| \mathbf{WAD}f(\tau_{11}) - D\mathbf{d} \|_{2}^{2}$$
 (61)

where Dd is the difference in the seismic data observed at baseline time and monitor survey time. From Eqs. (50)–(61), the horizontal principal stress can be acquired with at least single angle-stack observed seismic data. The change in horizontal stress is estimated from the objective function / with the iterative least-squares method in this study.

4. Synthetic examples

4.1. 1D case

We consider a relatively simple 1D stratigraphic model to test the proposed AVO inversion method. The SOE moduli (P-wave and S-wave velocities and density) and TOE moduli (c_{111} , c_{112} and c_{123}) of the unstressed 1D model at the baseline time are shown in

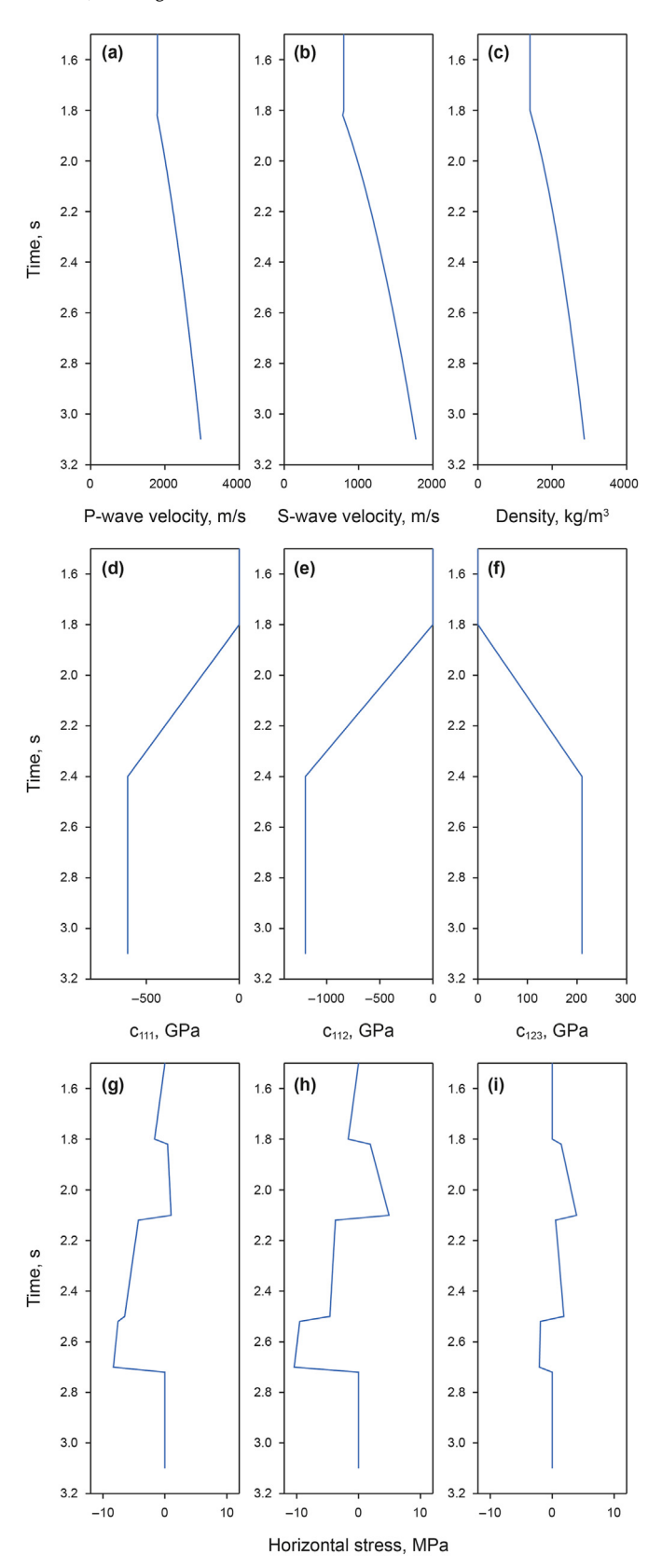


Fig. 3. 1D stratigraphic model: (a)—(c) SOE moduli; (d)—(f) TOE moduli; (g)—(h) horizontal stress at monitor survey times T_i and T_j ; (i) the change in horizontal stress between the baseline and the monitor survey time.

Fig. 3a-3f. Fig. 3g and h shows the distributions of horizontal stress at baseline time and monitor survey time, respectively. Fig. 3i shows the change in horizontal stress from baseline to monitor survey time. P- and S-wave velocities and density variation with horizontal stress are shown in Fig. 4a—c and the horizontal-stress-induced anisotropy parameters are shown in Fig. 4d—f.

Considering the properties of the 1D model, we use Eas. (27)–(33) to compute the reflection coefficients of P. SV and SH waves. Then the corresponding seismic data can be obtained with the convolution between the computed reflection coefficients and a minimum-phase wavelet with the dominant frequency of 25 Hz. Fig. 5a-5e show the P-wave seismic response with the azimuth of 10° (here the azimuth of 10° do not have any special meaning. Theoretically, the angle gathers at other azimuths are appropriate as well), SV-wave seismic response with the azimuth of 0°, SV-wave seismic response with the azimuth of 90°, SH-wave seismic response with the azimuth of 0° and SH-wave seismic response with the azimuth of 90° at baseline time T_i , monitor times T_i and T_k , respectively. The incident angles in all seismic responses range from 10° to 30° with the interval of 10°. From Fig. 5, we observe that the weak seismic reflection response exists at around 2.1 s when the model is unstressed, while the strong reflection response occurs in the model subjected to horizontal stress. The main reason is that the effects of horizontal stress on the properties of two media across 2.1 s are different, generating a strong impedance contrast across 2.1 s. We utilize D1-D6 to estimate the change in horizontal stress from the multi-wave (P-, SH- and SV-wave) time-lapse seismic responses with the incident angle spanning from 10° to 30° (as shown in Fig. 6a-f). Three angle seismic records are jointly used as input data to render a more stable inversion result. Fig. 7 displays the corresponding errors of the estimated results. From Figs. 6–7, we can see that relatively reasonable results can be obtained from P-wave, 0°-azimuth-SV-wave, 0°-azimuth-SH-wave and 90°-azimuth-SH-wave data with D1, D2, D4 and D5, while D3 and D6 provide the estimated results with large bias. Besides, the change in horizontal stress estimated from the P-wave time-lapse seismic data with three incident angles shows the most reasonable agreement with the real stress model. Moreover, compared with SV- and SH-wave responses, P-wave seismic response is easier to obtain in field production due to the widely used P-wave seismic excitation and acquisition. Therefore, at the current stage, the proposed AVO inversion method incorporating the information of the P wave has better potential for practical application. Because the change in horizontal stress and the original elastic parameters at the baseline time are known in this ideal 1D model, the reasonable inversion result is not able to totally imply the feasibility of the proposed method. The more complex synthetic example based on the observed seismic data should be further implemented to validate it, and the more technical details should be mentioned to ensure the proposed method can be easily applied in the field production.

4.2. 2D case

We implement the proposed inversion method incorporating P-wave seismic data (D1) in a 2D case to further test it. The target area is dominated by delta sediments and medium-grained sandstone with high porosity, which locates in Shengli oil field. A set of seismic data processing operations, including static correction and amplitude preserving, is implemented to ensure that the amplitudes of seismic data represent the strength of the reflection signals generated by subsurface interfaces as possible, as shown in Table 2. Based on Rüger reflection coefficient equation (Eq. (17)), to invert the original elastic and anisotropy parameters at the baseline time, the multi-azimuth or multi-angle original P-wave seismic data at the baseline time is necessary (Multi-angle seismic data is used in

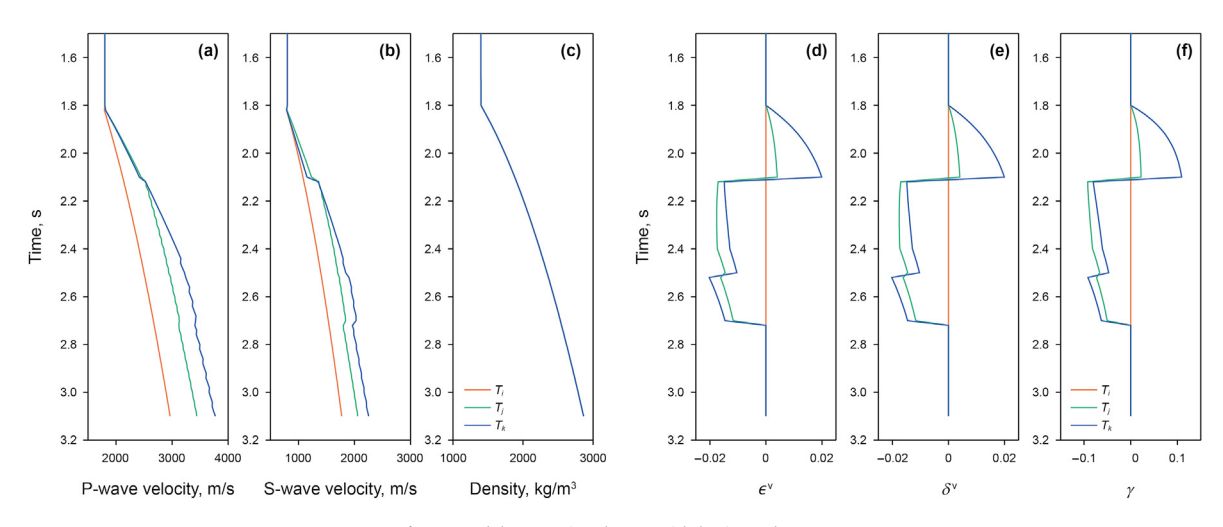


Fig. 4. Model properties change with horizontal stress.

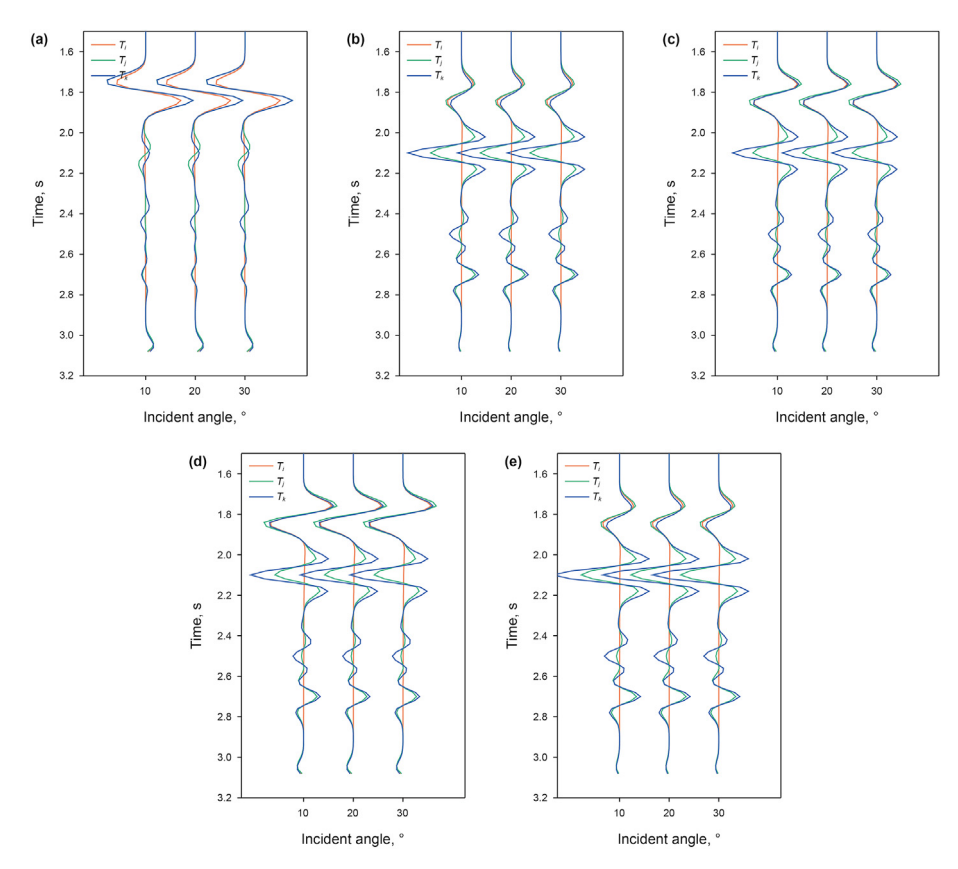


Fig. 5. Reflection responses of different waves at baseline T_i and monitor survey times T_j and T_k : (a) P wave with the azimuth of 10° ; (b) SV wave with the azimuth of 90° ; (c) SV wave with the azimuth of 90° ; (d) SH wave with the azimuth of 90° .

1D case, see Fig. 5a). The seismic data with the azimuths of 15° , 45° , 75° , 105° , 135° and 165° at incident angle 10° at the baseline time (shown in Fig. 8) is used to invert the original elastic and anisotropy parameters.

Figs. 9 and 10 display the elastic parameters (P-wave velocity, S-wave velocity and density) and Thomsen anisotropy parameters ($\delta^{(v)}$ and γ) which are inverted from the multi-azimuth seismic data with Rüger reflection coefficient equation in terms of P-wave velocity, S-wave velocity, density and anisotropy parameters. With the inverted elastic and anisotropy parameters, the original

overburden pressure can be computed with the product of gravity acceleration and the integral of density over the depth (Eq. (10) in Ma et al., 2017). Then the original horizontal stress at the baseline time can be straightforward calculated with Eq. (24) in Ma et al. (2017). The monitoring multi-azimuth seismic data at the monitor survey time is simulated by convolving P-wave reflection coefficients from Rüger reflection coefficient equation in terms of the changed P-wave velocity, S-wave velocity, density and anisotropy parameters and minimum-phase wavelet. We simulate the monitoring seismic data with 25% variation in the original

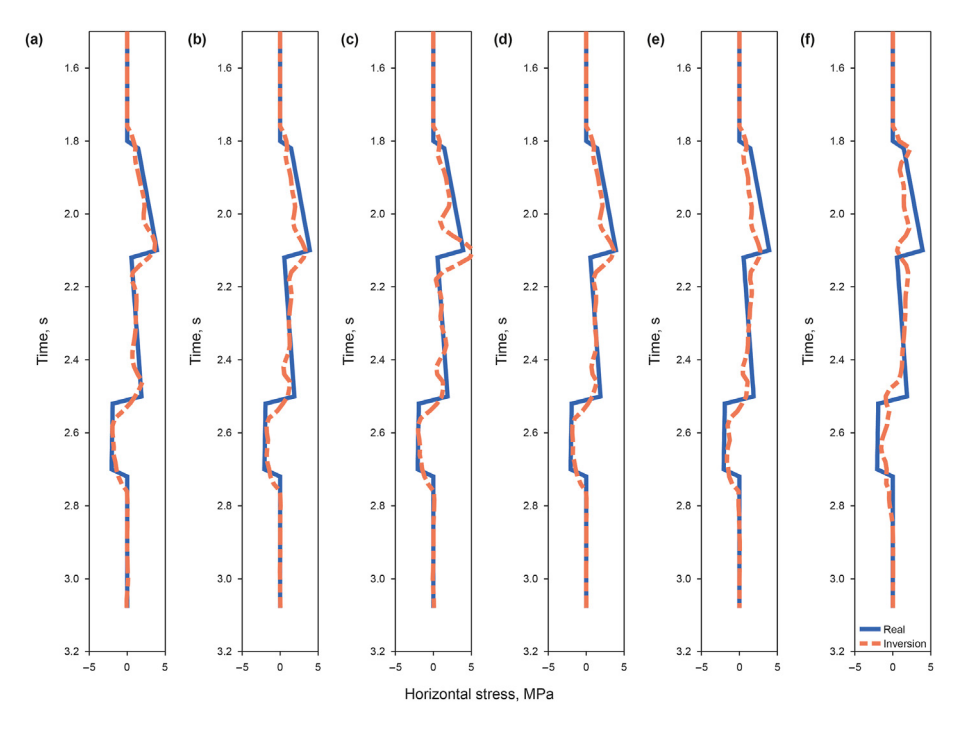


Fig. 6. Comparison between the changes in horizontal stress estimated from the time-lapse reflection responses shown in Fig. 5 with D1-D6 and the real model: (a) D1; (b) D2; (c) D3; (d) D4; (e) D5; (f) D6.

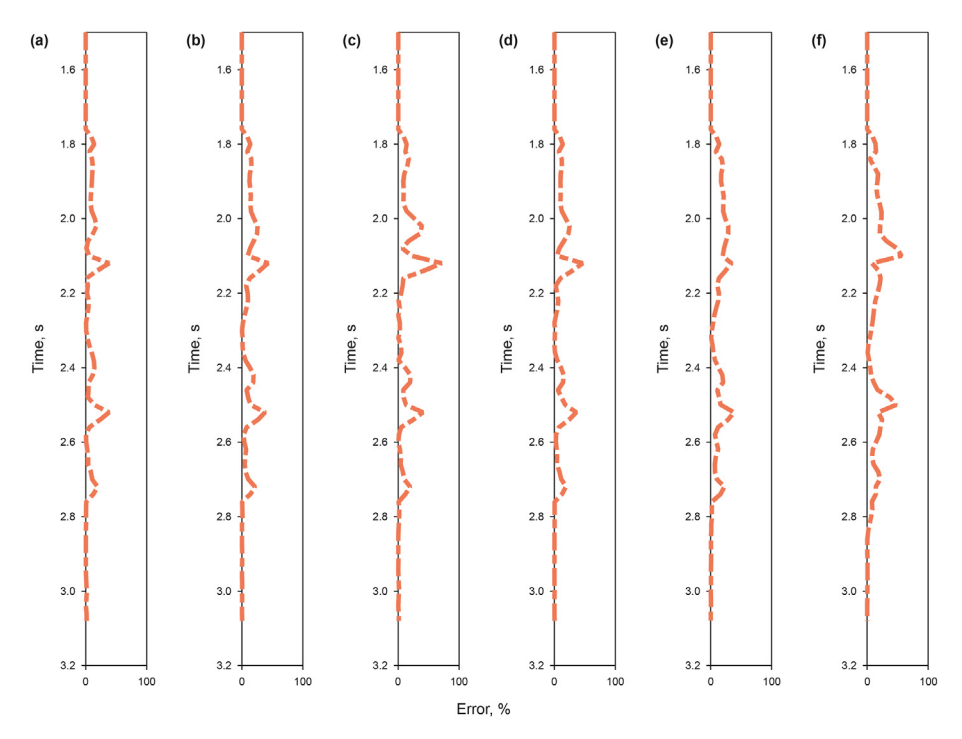


Fig. 7. The errors of stress results estimated by (a) D1; (b) D2; (c) D3; (d) D4; (e) D5; (f) D6, from the real model.

Table 1The second-order and third-order elastic constants of four rock samples after Winkler and McGowan (2004).

Rock	P-wave velocity, m/s	S-wave velocity, m/s	Density, kg/m ³	C ₁₁₁ , GPa	C ₁₁₂ , GPa	C ₁₂₃ , GPa
Rock 1	2127	1418	2062	-9550	-1370	1062
Rock 2	2183	1457	2120	-17038	-3273	-3160
Rock 3	2300	1640	2140	-13904	533	481
Rock 4	2037	1334	2080	-29106	-6940	-2090

Table 2Workflow for seismic data processing.

- 1. Trace editing and regulation
- 2. Static correction
- 3. Pre-stack muting
- 4. Pre-stack preserved-amplitude processing
- 5. Pre-stack deconvolution
- 6. Sort common mid-point (CMP) gathers
- 7. Velocity analysis
- 8. Normal moveout (NMO)
- 9. Pre-stack time migration
- 10. Post-stack deconvolution
- 11. Random noise attenuation
- 12. Inverse NMO
- 13. New velocity picking
- 14. NMO with new velocities
- 15. Transform to time-angle domain

horizontal stress, and the variations in P-wave velocity, S-wave velocity, density and anisotropy parameters can be further computed by Eqs. (12), (13) and (16). Fig. 11 displays the profile of the 25% change in original horizontal stress variation with the offset. The estimated result of the change in horizontal stress is displayed in Fig. 12. Compared Figs. 11 and 12, we observe that the estimated result shows a reasonable agreement with the real stress model and distinguishes the abnormal low-pressure and high-pressure areas. The negative sign of stress represents compressive stress. The rational lateral continuity in the profile of the estimated change in horizontal stress also illustrates the feasibility of the proposed approach in 2D or even 3D cases.

5. Discussion

In many engineering activities, such as gas and oil exploration, geothermal development and CO₂ injection and storage, the effects

of the changes in pore fluid (saturation) and stress on rock elasticity and seismic responses are coupling. The existing empirical and semi-quantitative approaches predict the relative change in in-situ stress using additional fitting parameters which can be determined with the prior well-logging data and rock physics analysis (Landrø, 2001: Trani et al., 2011: Lang and Grana, 2019), Despite considerable progress, how to fully quantify the relative change in stress from the observed seismic data remains to be elucidated. In order to overcome this problem, in this study, we used the nonlinear elasticity theory to describe the stress-dependent rock overall elastic properties. This theory regards the rock skeleton (solid phase) and pore fluid as an effective whole, which allows us not to consider the fluid variation because the fluid phase belongs to the overall rock system. Then, combining the nonlinear elasticity theory, seismic reflection theory and stress-induced anisotropy model, an AVO method to estimate the change in horizontal stress from observed P-, SV- and SH-wave reflection data are proposed. In 2D case example, we simulate the monitoring seismic data with the 25% variation in the original stress field. A similar operation was implemented by Zong et al. (2015) to validate the feasibility of the inversion method for the change in fluid factor. Although the reasonable agreement between the result of the change in horizontal stress estimated from P-wave seismic data and the given stress change can validate the proposed inversion approach, the relevant SV- and SH-wave field data should be applied to further validate the proposed approach in the future.

Eqs. (44)—(49) reveal the natural link between the change in horizontal principal stress and the variation in multi-wave (P-, SV- and SH-wave) seismic signals that help better understand the changes in subsurface structure and general fluid connectivity. Besides, the estimated results can provide new prior information for drilling. However, the derived wave reflection coefficient equation in horizontal-stress-induced anisotropic (HTI) media (Eqs. (17)—(21) combining Eqs. (9)—(15)) are not easy to be verified by us

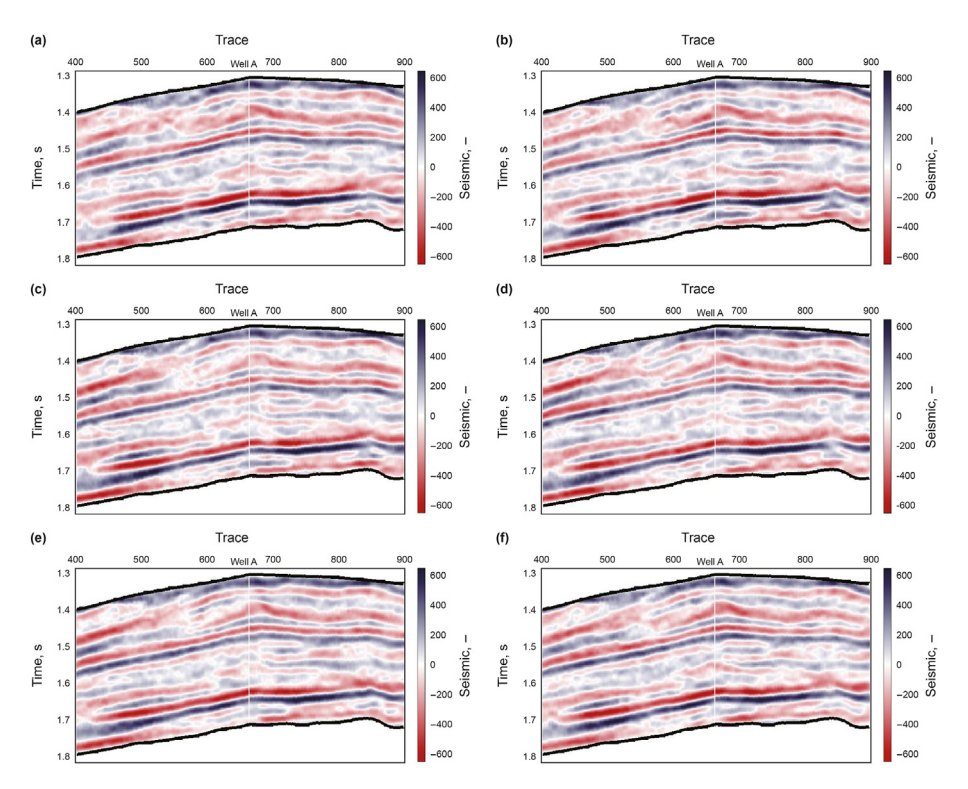


Fig. 8. Seismic profiles with the incident angle of 10° at baseline time: (a) Azimuth of 15°; (b) Azimuth of 45°; (c) Azimuth of 75°; (d) Azimuth of 105°; (e) Azimuth of 135°; (f) Azimuth of 165°.

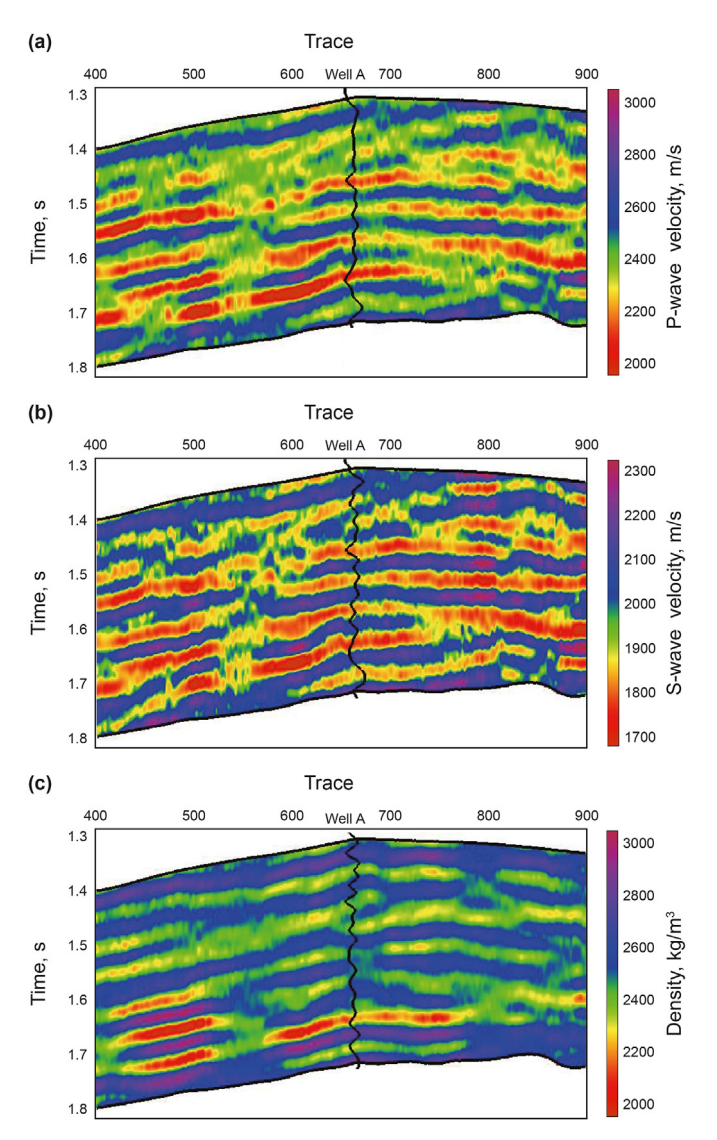


Fig. 9. The profiles of original elastic parameters at baseline time: (a) P-wave velocity; (b) S-wave velocity; (c) Density.

due to the unavailable laboratory excited and reflected waveforms in the horizontal-stress-induced HTI media. The relevant laboratory validation will be one of our research topics in the future. Moreover, the proposed reflection coefficient equations and inversion equations for change in horizontal stress may be not suitable in heterogeneous media such as the porous medium and fractured medium. This is because the nonlinear elasticity theory mentioned in this study is only suitable in homogeneous isotropic media. To monitor the changes in in-situ stress in more complex media, the

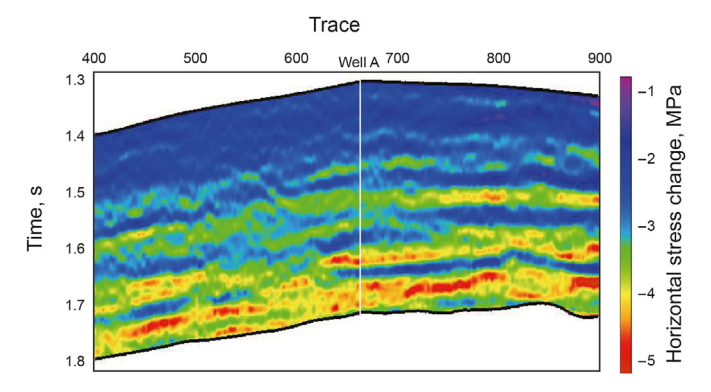


Fig. 11. The original profile of the change in horizontal stress.

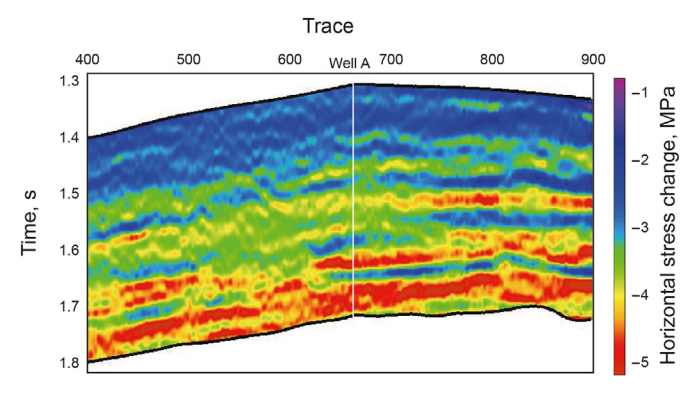


Fig. 12. The estimated profile of the change in horizontal stress.

generalized nonlinear elasticity theory should be developed. In addition, the seismic time shifts caused by stress changes are not considered even though such effects are inevitably encountered in field productions (Trani et al., 2011).

This study aims in illustrating the potential for estimating horizontal principal stress from the multi-wave time-lapse seismic responses with the proposed AVO inversion method. Therefore, we ideally neglect the effect of change in pore fluid on the wave reflection coefficients. The nature of the used nonlinear elasticity theory (i.e., regarding the real fluid-saturated porous rock as a whole system) ensures our study aim achieve. However, if people want to predict the changes in the in-situ stress and pore fluid from time-lapse seismic data, the classic nonlinear elasticity theory is incapable. The poro-acoustoelasticity theory (Ba et al., 2013) and pore structure model proposed by David and Zimmerman (2012) should be considered to generalize the proposed method to incorporate the joint effects of changes in in-situ stress and pore fluid on the reflection coefficients or seismic reflection signatures in the future study.

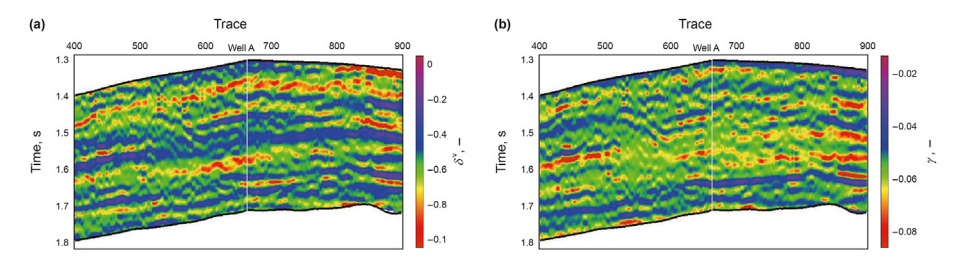


Fig. 10. The profiles of original anisotropy parameters at baseline time: (a) $\delta^{(\nu)}$; (b) γ .

6. Conclusions

A physically based approach is proposed to estimate the change in horizontal principal stress from the P-wave, SV-wave, and SHwave time-lapse reflection data. Compared with the conventional methods, the proposed approach eliminates the need for additional empirical or fitting coefficients, rendering the more stable estimated results. 1D model test illustrates the feasibility of the proposed approach for estimating horizontal stress from six different wave responses, and the 2D synthetic case further illustrates the feasibility of the approach for inverting horizontal stress from Pwave seismic data. Besides, Eqs. (44)–(49) describe the relationship between the changes in horizontal stress and time-lapse seismic responses, and provide the theoretical reference for estimating the changes in biaxial stress and even confining stress with the joint information of multi waves in field production. Our results are relevant to CO₂ injection and storage, gas and oil exploration and geothermal development in the subsurface Earth.

Acknowledgement

The authors acknowledge the sponsorship of National Natural Science Foundation of China (42174139, 41974119, 42030103), Laoshan Laboratory Science and Technology Innovation Program (LSKJ202203406), and Science Foundation from Innovation and Technology Support Program for Young Scientists in Colleges of Shandong Province and Ministry of Science and Technology of China (2019RA2136).

References

- Ba, J., Carcione, J.M., Cao, H., et al., 2013. Poro-acoustoelasticity of fluid-saturated rocks. Geophys. Prospect. 61 (3), 599–612. https://doi.org/10.1111/j.1365-2478.2012.01091.x.
- Cai, C., Li, B.R., Zhang, Y.Y., et al., 2022. Fracture propagation and induced strain response during supercritical CO₂ jet fracturing. Petrol. Sci. https://doi.org/10.1016/j.petsci.2022.03.019.
- Chen, F.B., Zong, Z.Y., Jiang, M., 2021. Seismic reflectivity and transmissivity parameterization with the effect of normal in-situ stress. Geophys. J. Int. 226 (3), 1599–1614. https://doi.org/10.1093/gji/ggab179.
- Chen, F.B., Zong, Z.Y., Yin, X.Y., 2022a. Acoustothermoelasticity for joint effects of stress and thermal fields on wave dispersion and attenuation. J. Geophys. Res. Solid Earth 127 (4), e2021 B023671. https://doi.org/10.1029/2021 B023671.
- Chen, F.B., Zong, Z.Y., Yin, X.Y., et al., 2022b. Accurate formulae for P-wave reflectivity and transmissivity for a non-welded contact interface with the effect of in situ vertical stress. Geophys. J. Int. 229 (1), 311–327. https://doi.org/10.1093/gji/ggab475.
- David, E.C., Zimmerman, R.W., 2012. Pore structure model for elastic wave velocities in fluid-saturated sandstones. J. Geophys. Res. 117 (B7), B07210. https://doi.org/ 10.1029/2012/B009195.
- Degtyar, A.D., Rokhlin, S.I., 1998. Stress effect on boundary conditions and elastic wave propagation through an interface between anisotropic media. J. Acoust. Soc. Am. 104 (4), 1992–2003. https://doi.org/10.1121/1.423765.
- Grude, S., Landrø, M., 2012. Time Lapse Pressure-Saturation Discrimination for CO₂
 Storage at the Snøhvit Field. SEG Technical Program Expanded Abstracts, pp. 4609–4614. https://doi.org/10.1016/j.ijggc.2013.09.014.
- House, K.Z., Schrag, D.P., Harvey, C.F., et al., 2006. Permanent carbon dioxide storage in deep-sea sediments. Proc. Natl. Acad. Sci. USA 103 (33), 12291–12295. https://doi.org/10.1073/pnas.0605318103.
- Hughes, D.S., Kelly, J.L., 1953. Second-order elastic deformation of solids. Phys. Rev. 92 (5), 1145–1149. https://doi.org/10.1103/PhysRev.92.1145.
- Johnson, P.A., Rasolofosaon, P., 1996. Nonlinear elasticity and stress-induced anisotropy in rock. J. Geophys. Res. 101 (B2), 3113–3124. https://doi.org/ 10.1029/95/B02880.
- Landrø, M., 2001. Discrimination between pressure and fluid saturation changes from time-lapse seismic data. Geophysics 66 (3), 836–844. https://doi.org/ 10.1190/1.1444973.
- Lang, X.Z., Grana, D., 2019. Rock physics modelling and inversion for saturationpressure changes in time-lapse seismic studies. Geophys. Prospect. 67 (7),

- 1912-1928. https://doi.org/10.1111/1365-2478.12797.
- Li, J., Chen, Z.Y., Feng, Y.C., et al., 2022. Damage of reservoir rock induced by CO2 injection. Petrol. Sci. https://doi.org/10.1016/j.petsci.2022.03.016.
- Liu, J.X., Cui, Z.W., Wang, K.X., 2012. Effect of stress on reflection and refraction of plane wave at the interface between fluid and stressed rock. Soil Dynam. Earthq. Eng. 42, 47–55. https://doi.org/10.1016/j.soildyn.2012.05.022.
- Liu, J.X., Cui, Z.W., Wang, K.X., et al., 2017. Determining maximum shear stress in confined substrate from elastic wave reflection coefficient. Sci. China Earth Sci. 60 (6), 1147–1158 https://doi.org/CNKI:SUN:JDXG.0.2017-06-010.
- Ma, N., Yin, X.Y., Sun, C.Y., et al., 2017. The in-situ stress seismic prediction method based on the theory of orthorhombic anisotropic media. Chin. J. Geophys. 60 (12), 4766–4775. https://doi.org/10.6038/cjg20171218 (in Chinese).
- Masumi, H., Matsumura, J., Ryoichi, K., et al., 2010. Acoustoelastic effect in Melia azedarach for nondestructive stress measurement. Construct. Build. Mater. 24 (9), 1713–1717. https://doi.org/10.1016/j.conbuildmat.2010.02.018.
- Meadows, M., 2001. Enhancements to Landro's Method for Separating Time-Lapse Pressure and Saturation Changes. SEG Technical Program Expanded Abstracts, pp. 1652–1655. https://doi.org/10.1190/1.1816433.
- Nur, A., Simmons, G., 1969. Stress-induced velocity anisotropy in rock: an experimental study. J. Geophys. Res. 74, 6667–6674. https://doi.org/10.1029/IB074i027p06667.
- Pao, Y.H., Sachse, W., Fukuoka, H., 1984. Acoustoelasticity and Ultrasonic Measurement of Residual Stress. Physical Acoustics. Mason W.P, Thurston R.N, Publisher
- Rasolofosaon, P., 1998. Stress-induced seismic anisotropic revisited. Rev. Inst. Fr. Petrol 53 (5), 679–692. https://doi.org/10.2516/ogst:1998061.
- Rojas, E., Davis, T.L., Batzle, M., et al., 2005. Vp-Vs Sensitivity to Pressure, Fluid, and Lithology Changes in Tight Gas Sandstones. SEG Technical Program Expanded Abstracts, pp. 1401–1404. https://doi.org/10.1190/1.2147950.
- Rüger, A., 1996. Analytic Insight into Shear-Wave AVO for Fractured Reservoirs. SEG
 Technical Program Expanded Abstracts, pp. 1801–1804. https://doi.org/10.1190/
- Rüger, A., 1998. Variation of P-wave reflectivity with offset and azimuth in anisotropic media. Geophysics 63 (3), 935–947. https://doi.org/10.1190/1.1444405.
- Sarkar, D., Bakulin, A., Kranz, R., 2003. Anisotropic inversion of seismic data for stressed media: theory and a physical modeling study on Berea Sandstone. Geophysics 68 (2), 690–704. https://doi.org/10.1190/1.1567240.
- Shapiro, S.A., 2017. Stress impact on elastic anisotropy of triclinic porous and fractured rocks. J. Geophys. Res. Solid Earth 122 (3), 2034–2053. https://doi.org/ 10.1002/2016jb013378.
- Sripanich, Y., Vasconcelos, I., Tromp, J., et al., 2021. Stress-dependent elasticity and wave propagation—new insights and connections. Geophysics 86 (4), W47—W64. https://doi.org/10.1190/geo2020-0252.1.
- Stovas, A., Landrø, M., 2004. Optimal use of PP and PS time-lapse stacks for fluid pressure discrimination. Geophys. Prospect. 52 (4), 301–312. https://doi.org/ 10.1111/i.1365-2478.2004.00420.x.
- Thomsen, L., 1986. Weak elastic anisotropy. Geophysics 51 (10), 1954–1966. https://doi.org/10.1190/1.1442051.
- Thurston, R.N., Brugger, K., 1964. Third-order elastic constants and the velocity of small amplitude elastic waves in homogeneously stressed media. Phys. Rev. 133 (6A), A1604—A1610. https://doi.org/10.1103/physrev.133.a1604.
- Trani, M., Arts, R., Leeuwenburgh, O., et al., 2011. Estimation of changes in saturation and pressure from 4D seismic AVO and time-shift analysis. Geophysics 76 (2), C1–C17. https://doi.org/10.1190/1.3549756.
- Tromp, J., Trampert, J., 2018. Effects of induced stress on seismic forward modelling and inversion. Geophys. J. Int. 213 (2), 851–867. https://doi.org/10.1093/gji/ggy020.
- Tsvankin, I., 1997. Anisotropic parameters and P-wave velocity for orthorhombic media. Geophysics 62 (4), 1292–1309. https://doi.org/10.1190/1.1444231.
- Tura, A., Lumley, D.E., 1999. Estimating Pressure and Saturation Changes from Time Lapse AVO Data. SEG Technical Program Expanded Abstracts, pp. 1655–1658. https://doi.org/10.1190/1.1820849.
- Winkler, K.W., McGowan, L., 2004. Nonlinear acoustoelastic constants of dry and saturated rocks. J. Geophys. Res. 109 (B10), 1–9. https://doi.org/10.1029/2004IB003262.
- Witsker, S.O.S., Landrø, M., Avseth, P., 2014. Using a pseudo-steady-state flow equation and 4D seismic travel-time shifts for estimation of pressure and saturation changes. Geophysics 79 (3), M11–M24. https://doi.org/10.1190/GF02013-02471.
- Wong, M.Y., 2017. Pressure and Saturation Estimation from PRM Time-Lapse Seismic Data for a Compacting Reservoir. Doctoral Thesis. Heriot-Watt University, Edinburgh, UK.
- Zong, Z.Y., Ji, L.X., 2021. Model parameterization and amplitude variation with angle and azimuthal inversion in orthotropic media. Geophysics 86 (1), 1JF–V89. https://doi.org/10.1190/geo2018-0778.1.
- Zong, Z.Y., Yin, X.Y., Wu, G.C., et al., 2015. Elastic inverse scattering for fluid variation with time-lapse seismic data. Geophysics 80 (2), WA61—WA67. https://doi.org/10.1190/GEO2014-0183.1.